

Article

Equilibrium, Kinetic, and Thermodynamic Studies on Adsorption of Rhodamine B from Aqueous Solutions Using Oxidized Mesoporous Carbons

Michał Marciniak¹, Joanna Goscińska¹, Małgorzata Norman², Teofil Jesionowski², Aleksandra Bazan-Wozniak¹ and Robert Pietrzak^{1,*}

¹ Faculty of Chemistry, Adam Mickiewicz University in Poznań, Uniwersytetu Poznańskiego 8, 61-614 Poznań, Poland

² Faculty of Chemical Technology, Poznań University of Technology, Berdychowo 4, 60-965 Poznań, Poland

* Correspondence: pietrob@amu.edu.pl; Tel.: +48-61-829-1560

Abstract: Oxidized mesoporous carbon C_{SBA-15}, obtained by the hard method, was applied to remove rhodamine B from the aqueous system. The process of carbon oxidation was performed using 0.5 and 5 M of nitric (V) acid solution at 70 and 100 °C. Functionalization of mesoporous carbon with HNO₃ solutions led to reduction in the surface area, pore volume, and micropore area, however, it also led to an increased number of oxygen functional groups of acidic character. The functional groups probably are located at the entrance of micropores, in this way, reducing the values of textural parameters. Isotherms of rhodamine B adsorption indicate that the oxidation of mesoporous carbons resulted in an increase in the effectiveness of the removal of this dye from aqueous solutions. The influence of temperature, pH, and contact time of mesoporous material/rhodamine B on the effectiveness of dye removal was tested. The process of dye adsorption on the surfaces of the materials studied was established to be most effective at pH 12 and at 60 °C. Kinetic studies of the process of adsorption proved that the equilibrium state between the dye molecules and mesoporous carbon materials is reached after about 1 h. The adsorption kinetics were well fitted using a pseudo-second-order model. The most effective in rhodamine B removal was the sample C_{SBA-15-5-100}, containing the greatest number of oxygen functional groups of acidic character. The Langmuir model best represented equilibrium data.

Keywords: ordered mesoporous carbons; hexagonal structure; hard template method; oxidation by nitric acid; cationic dye; adsorption



Citation: Marciniak, M.; Goscińska, J.; Norman, M.; Jesionowski, T.; Bazan-Wozniak, A.; Pietrzak, R. Equilibrium, Kinetic, and Thermodynamic Studies on Adsorption of Rhodamine B from Aqueous Solutions Using Oxidized Mesoporous Carbons. *Materials* **2022**, *15*, 5573. <https://doi.org/10.3390/ma15165573>

Academic Editor: Antonio Gil Bravo

Received: 1 July 2022

Accepted: 10 August 2022

Published: 13 August 2022

Publisher's Note: MDPI stays neutral with regard to jurisdictional claims in published maps and institutional affiliations.



Copyright: © 2022 by the authors. Licensee MDPI, Basel, Switzerland. This article is an open access article distributed under the terms and conditions of the Creative Commons Attribution (CC BY) license (<https://creativecommons.org/licenses/by/4.0/>).

1. Introduction

Water, which is the element necessary to support all forms of life, covers most of Earth's surface. Its pollution is negative to human health and the entire hydrosphere [1–5]. There is a constant increase in the content of organic compounds in wastewater, especially in post-production waste produced by different types of industry [6,7], such as the textile industry, reaching several thousand tons a year, of which 10–20% is lost in the process of production [8–10]. Dyes are usually well soluble in water and resistant to degradation by various methods (biological, physical, and chemical) [9–12]. Therefore, they must be removed from the wastewater. At present, a few methods are used to remove organic compounds [12–14]. From among newly proposed methods, very attractive seems to be the method of membrane separation, offering simplicity of operation and low energy consumption [15]. On the other hand, membrane efficiency decreases with time because of the fouling of pollutant particles on the membrane surface and inside membrane pores. Moreover, molecules of many organic compounds are smaller than the membrane pores and the process of membrane separation is ineffective [16–18]. Currently, the most effective are the adsorption methods that can be used for the removal of organic and inorganic

compounds from water solutions. The properties and quality of the adsorbent influence the adsorption efficiency. Many materials, for example, silica gels [19], alumina [20], and zeolite molecular sieves [21,22] are rather ineffective in the adsorption process. Activated carbons are used as organic pollutant adsorbents, although the presence of micropores in their structure limits the penetration of larger dye molecules into the pores. Recently, much attention was paid to ordered mesoporous carbon materials, as they show unique properties, such as thermal and mechanical stability, as well as good textural parameters [23]. These materials are easily modified, which allows for improved adsorption properties towards a range of pollutants [23–26]. Many methods for carbon material modification were proposed, but the most effective is that of wet oxidation, in which oxygen functional groups are introduced on the carbon surface [27]. A number of authors studied the adsorption of organic compounds on carbon materials, for instance, Liu et al. [28] proposed the removal of Acid Red 73 and Reactive Black 5 by CMK-3, CMK-5, and its carbon/silica composite Si-CMK-5, with different pore structures. The greatest sorption capacity towards these dyes was shown by CMK-5, which was related to double pore systems and large specific surface area. Asouhidou et al. [29] obtained mesoporous carbons, a highly ordered CMK-3 sample with hexagonal structure and a disordered mesoporous carbon (DMC), and tested them in the removal of Remazol Red 3BS, comparing their performance with that of commercial products (Takeda 5A, Calgon, and Norit SAE-2) and a HMS mesoporous silica with a wormhole pore structure. Their results show that the material structure and pore size have a significant impact on the effectiveness of adsorption. The resulting sorption capacities decreased in the order CMK-3 (0.531 mmol/g) > DMC (0.453 mmol/g) > SAE-2 (0.167 mmol/g) > Calgon (0.05 mmol/g) > Takeda 5A = HMS (0.007 mmol/g). The group of Peng [30] successfully applied the ordered mesoporous CMK-3 containing nitrogen functional groups as the adsorbent of Acid Black 1. According to their results, the modification of mesoporous carbon significantly improved its effectiveness in the removal of this dye. The maximum sorption capacities of the initial and functionalized materials were over 270 mg/g and nearly 500 mg/g, respectively.

One of the most popular textile dyes is rhodamine B, which is a cationic synthetic dye of green or red purple crystals [31]. With the release of rhodamine B into the water, several environmental and public health problems are caused [32,33]. Very popular and effective adsorbents of rhodamine B from water solutions are mesoporous carbons [34–36]. Therefore the aim of the study was to analyze the process of rhodamine B removal from water solutions by adsorption on oxidized mesoporous carbons of hexagonal structure. The effects of pH of the dye solution, adsorbent/adsorbate contact time, and temperature of the process were checked on the sorption capacity of obtained mesoporous carbons. The mesoporous carbon materials used as adsorbents were characterized in detail by a number of physicochemical methods.

2. Materials and Methods

2.1. Sample Preparation

2.1.1. Mesoporous Carbon Synthesis

Mesoporous carbon C_{SBA-15} was obtained by the hard template method using the ordered silica SBA-15 as the solid template and sucrose as the carbon precursor [37,38]. The substrates for SBA-15 preparation were 50 mg of Pluronic P123 (EO₂₀PO₇₀EO₂₀; Aldrich, Saint Louis, MO, USA), 19 mL of 1.6 M HCl (Avantor Performance Materials Poland S.A., Gliwice, Poland), and 1.1 mL of TEOS (MERCK KGaA, Darmstadt, Germany). Pluronic P123 was dissolved in a water solution of HCl at 35 °C. To the mixture, TEOS was added dropwise upon stirring continued for 6 h. Then the mixture was subjected to hydrothermal treatment in poly-propylene bottles in a drier (1 day at 35 °C and the next 6 h at 100 °C). Then the material obtained was filtered off and dried (100 °C, 12 h). The template was removed by calcination (550 °C, 8 h). The procedure produced ordered mesoporous silica SBA-15 of hexagonal structure [37,38]. The mesoporous silica SBA-15 was subjected to twice repeated impregnation using sucrose solution. Next, 125 mg sucrose (MERCK KGaA,

Darmstadt, Germany) was dissolved in H₂SO₄ (0.14 mL, Avantor Performance Materials Poland S.A., Gliwice, Poland) and 5 mL of distilled water. The solution was added to the flask with the ordered silica. The contents were heated in the oven (6 h at 100 °C and 6 h at 160 °C). The obtained material was subjected to another impregnation with a solution of sucrose (800 mg), H₂SO₄ (0.09 mL), and distilled water (5 mL).

The composite was then subjected to carbonization by heating for 2 h at 900 °C. The remaining silica was washed out twice with 5% of HF solution (200 mL, Avantor Performance Materials Poland S.A., Gliwice, Poland). The material was filtered off, washed with C₂H₅OH, and dried (12 h at 100 °C) [39].

2.1.2. Sample Functionalization

The C_{SBA-15} of the hexagonal structure was subjected to oxidation at 70 or 100 °C with the use of HNO₃ at the concentrations of 0.5 or 5 mol/L as the oxidizing agent. Next, 0.5 g of the carbon was placed in a round-bottomed flask and flooded with 30 mL of nitric (V) acid solution. Oxidation was performed under reflux (12 h). Next, the contents were filtered off and the carbon was washed with C₂H₅OH and distilled water. The oxidized carbon materials were labeled as C_{SBA-15}-0.5-70, C_{SBA-15}-5-70, C_{SBA-15}-0.5-100, and C_{SBA-15}-5-100, where 70 and 100 refer to the temperature of oxidation, while 0.5 and 5 to the concentration of HNO₃.

2.2. Analytical Procedures

The texture parameters of the samples obtained were characterized by low-temperature nitrogen adsorption/desorption isotherms measured on a sorptometer Quantachrome Autosorb iQ (Boynton Beach, FL, USA) [9].

X-ray diffraction patterns were obtained on a Bruker AXS DB Advance diffractometer (CuK_α radiation, λ = 0.154 nm, step size 0.02°).

The number of surface oxygen functional groups was determined by the Boehm method [40]. A portion of 0.25 g of adsorbent was placed in 25 mL of 0.1 mol/L solutions of either NaOH or HCl. The vials were sealed and shaken for 24 h and then 10 mL of each filtrate was pipetted and the excess of base or acid was titrated with 0.1 mol/L HCl or NaOH, as required. The numbers of acidic sites of various types were calculated assuming that NaOH neutralizes all acidic groups and HCl reacts with all basic groups.

Structural changes in the oxidized mesoporous carbon materials were determined by FT-IR spectroscopy. The preparation of samples is described in the paper [9]. The study was carried out on a Varian 640-IR spectrometer (Agilent, Santa Clara, CA, USA).

Zeta potential was determined using a Zetasizer Nano ZS instrument equipped with an autotitrator (Malvern Instruments Ltd., Malvern, United Kingdom) [41]. The electrophoretic mobility of the particles was measured and converted to the zeta potential according to the Henry Equation (1):

$$R_{ef} = \frac{2\varepsilon\zeta f(K_a)}{3\eta} \quad (1)$$

where R_{ef} is the electrophoretic mobility, ε the dielectric constant; ζ the electrokinetic (zeta) potential; η the viscosity, and $f(K_a)$ the Henry function. The isoelectric point is a pH value at which zeta potential is zero, the surface has net electrical neutrality. When $\text{pH} > i_{ep}$, the surface charge is negative and $\text{pH} < i_{ep}$, it is positive.

2.3. Adsorption of Rhodamine B

The carbon material portions of 0.02 g were placed in flasks and flooded with 50 mL of a dye solution of a given concentration (25–250 mg/L), and the contents were shaken at 22 ± 1 °C for 24 h. Spectrophotometric measurements were carried out with a spectrometer Cary 100 Bio (Agilent, Santa Clara, CA, USA). Rhodamine B absorbs the irradiation of

$\lambda_{\max} = 553$ nm. The amount of rhodamine B adsorbed on the oxidized mesoporous carbons was calculated from Equation (2):

$$q_e = \frac{C_0 - C_e}{m} \times V \quad (2)$$

where: C_0 —initial rhodamine B concentration (mg/L); C_e —equilibrium rhodamine B concentration (mg/L); m —the mass of mesoporous carbon sample (g); V —volume of rhodamine B solution (L). The experimental adsorption studies were carried out twice and are shown with a standard deviation error.

The effects of pH (CP-401 pH-meter, ELMETRON, Zabrze, Poland) of the dye solutions, temperature, and contact time of the sample/rhodamine B on the sorption capacities of mesoporous carbons were studied.

2.4. Adsorption Modeling

Experimental data were fitted to pseudo-first-order (3) and pseudo-second-order (4) models [9]:

$$\ln(q_e - q_t) = \ln q_e - \frac{k_1 t}{2.303} \quad (3)$$

where: q_e —sorption capacity of the rhodamine B adsorbed at equilibrium state (mg/g); q_t —sorption capacity of the rhodamine B adsorbed in time (mg/g); and k_1 —the rate constant for the pseudo-first order model (min^{-1}).

The pseudo-second-order model can be expressed by the equation:

$$\frac{t}{q_t} = \frac{1}{k_2 q_e^2} + \frac{t}{q_e} \quad (4)$$

where: k_2 —the rate constant for pseudo-second order model (g/mg·min).

2.5. Thermodynamic Study

Thermodynamic parameters [42–44] were calculated by using the following Equation (5):

$$\Delta G^0 = -RT \ln K_d \quad (5)$$

where: ΔG^0 —Gibbs free energy ($\text{J} \cdot \text{mol}^{-1}$); R —universal constant ($8.314 \text{ J} \cdot \text{mol}^{-1} \cdot \text{K}^{-1}$); T temperature (K); and K_d —thermodynamic equilibrium constant.

The Gibbs free energy of adsorption (ΔG^0) can be represented by the Equation (6):

$$\Delta G^0 = \Delta H^0 - T \Delta S^0 \quad (6)$$

where: ΔH^0 —enthalpy change; ΔS^0 —entropy change.

Thermodynamic parameters can be also calculated from Equation (7):

$$\ln K_d = \frac{\Delta S^0}{R} + \frac{\Delta H^0}{RT} \quad (7)$$

ΔH^0 and ΔS^0 parameters were calculated (7) from the slope and intercept of the plot of $\ln K_d$ versus $1/T$ yields, respectively.

2.6. Adsorption Isotherms

In our work, we used the Langmuir and Freundlich models to explain the mechanism of rhodamine B adsorption on oxidized carbon materials [45,46].

The linear equation of Langmuir isotherm (8) is represented as follows:

$$\frac{C_e}{q_e} = \frac{1}{K_L \times q_{\max}} + \frac{C_e}{q_{\max}} \quad (8)$$

where: C_e —equilibrium concentration of rhodamine B (mg/L); q_e —sorption capacity of rhodamine B adsorbed onto the adsorbent at equilibrium (mg/g); q_m —maximum monolayer adsorption capacity of adsorbent (mg/g); and K_L —Langmuir adsorption constant (L/mg).

The Freundlich isotherm is expressed mathematically as [46] (9):

$$\ln q_e = \ln K_F + \frac{1}{n} \ln C_e \quad (9)$$

where: q_e —sorption capacity of rhodamine B adsorbed at equilibrium (mg/g); C_e —equilibrium concentration of rhodamine B (mg/L); K_F —Freundlich adsorption constant (mg/g · (L/mg)^{1/n}); and n —Freundlich constant indicates how favorable the adsorption process is.

Experimental data were also fitted to the non-linear Langmuir and Freundlich models.

3. Results and Discussion

3.1. Characterization of Adsorbents

The data on textural parameters are presented in Table 1. The sample of C_{SBA-15} is characterized by a well-developed surface area ($S_{\text{BET}} = 1203 \text{ m}^2/\text{g}$) and a total pore volume (V_t) of $1.32 \text{ cm}^3/\text{g}$. The carbon obtained in this way also has micropores, whose area (S_{micro}) is $682 \text{ m}^2/\text{g}$. The process of functionalization of sample C_{SBA-15} leads to a decrease in these parameters. However, the changes are not uniform and depend on the conditions of the oxidation process. Although sample C_{SBA-15-5-100} was obtained by treatment with a 5 mol/L solution of HNO₃ at 100 °C, it shows the largest surface area from among all oxidized materials ($854 \text{ m}^2/\text{g}$). The micropore area and total pore volume of this material are $198 \text{ m}^2/\text{g}$ and $1.10 \text{ cm}^3/\text{g}$, respectively. Most probably in the conditions applied (100 °C, 5 mol/L HNO₃), the micropores are unblocked again and the carbon compounds are removed, which increases the micropore area and total surface area [47]. The smallest S_{BET} of $685 \text{ m}^2/\text{g}$, S_{micro} of $106 \text{ m}^2/\text{g}$, and V_t of $0.89 \text{ cm}^3/\text{g}$ were obtained for sample C_{SBA-15-5-70}. The reduced values of textural parameters are most probably caused by the localization of the newly generated oxygen functional groups in micropores, which leads to their blocking and decreases the surface area.

Table 1. Textural parameters of adsorbents obtained ¹.

| Adsorbent | S_{BET} (m ² /g) | V_t (cm ³ /g) | S_{micro} (m ² /g) | Average Pore Diameter (nm) |
|-----------------------------|--------------------------------------|----------------------------|--|----------------------------|
| C _{SBA-15} | 1203 | 1.32 | 685 | 4.45 |
| C _{SBA-15-0.5-70} | 789 | 1.12 | 147 | 5.66 |
| C _{SBA-15-5-70} | 685 | 0.89 | 106 | 5.18 |
| C _{SBA-15-0.5-100} | 837 | 1.04 | 204 | 4.91 |
| C _{SBA-15-5-100} | 854 | 1.10 | 198 | 5.18 |

¹ Error range between 2% and 5%.

Recorded in the small angle range XRD, diffractograms of the adsorbents obtained are depicted in Figure 1. Diffractograms of all samples show one intensive peak characteristic of hexagonal pore arrangement [9]. The diffractograms of the initial material C_{SBA-15} and samples C_{SBA-15-0.5-100} and C_{SBA-15-5-100} contain also the reflections in the range $2\theta \approx 1.7\text{--}2.5^\circ$, corresponding to the planes (100), (110), and (200) of P6 mm structure, evidencing good ordering of the materials. No analogous reflections are observed for C_{SBA-15-0.5-70} and C_{SBA-15-5-70}, which indicates a partial disturbance in the mesoporous structure.

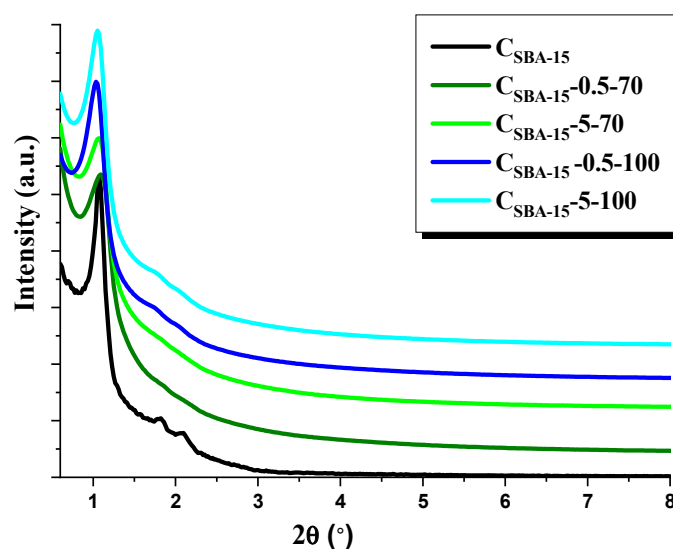


Figure 1. XRD patterns of adsorbents obtained.

Table 2 presents the results obtained from Boehm titration. The oxidation of mesoporous sample C_{SBA-15} with a solution of HNO_3 generates on its surface acidic functional groups whose content depends on the conditions of the process. When using 0.5 mol/L and 5 mol/L HNO_3 solution, the content of basic groups decreased to 0.13 mmol/g for samples $C_{SBA-15-0.5-70}$ and $C_{SBA-15-0.5-100}$, and to their total disappearance on samples $C_{SBA-15-5-70}$ and $C_{SBA-15-5-100}$. For the acidic functional groups, the results are different. The content of acidic groups in the initial carbon material C_{SBA-15} is 1.09 mmol/g. The content of such groups increases after oxidation and clearly depends on the functionalization conditions, which are the concentration of nitric (V) acid and process temperature. The highest content of the acidic functional groups of 4.88 mmol/g was observed for the sample oxidized with 5 mol/L HNO_3 solution at 100 °C ($C_{SBA-15-5-100}$). Reduction in the temperature of the process or in the concentration of the oxidizing agent led to lower content of acidic surface functional groups: $C_{SBA-15-0.5-70}$ –2.14 mmol/g, $C_{SBA-15-5-70}$ –3.24 mmol/g, and $C_{SBA-15-0.5-100}$ –3.45 mmol/g.

Table 2. The results obtained from Boehm titration.

| Adsorbent | Acidic Groups (mmol/g) | Basic Groups (mmol/g) | Total Content of Acidic and Basic Groups (mmol/g) |
|----------------------|------------------------|-----------------------|---|
| C_{SBA-15} | 1.09 ± 0.01 | 0.74 ± 0.01 | 1.83 |
| $C_{SBA-15-0.5-70}$ | 2.14 ± 0.02 | 0.13 ± 0.01 | 2.27 |
| $C_{SBA-15-5-70}$ | 3.24 ± 0.02 | 0.00 ± 0.00 | 3.24 |
| $C_{SBA-15-0.5-100}$ | 3.45 ± 0.02 | 0.13 ± 0.01 | 3.58 |
| $C_{SBA-15-5-100}$ | 4.88 ± 0.03 | 0.00 ± 0.00 | 4.88 |

Figure 2 presents the transmission FT-IR spectra of the initial carbon C_{SBA-15} and oxidized samples of acidic surface nature.

The FT-IR spectra show a rather broad band at about 1200 cm^{-1} that can be assigned to the stretching vibrations of the C–O bond in ethers, acid anhydrides, or phenol. The bands about 1600 cm^{-1} correspond to the stretching vibrations of carbon–carbon bonds in the aromatic ring. There is also a clearly visible band at 3400 cm^{-1} , assigned to the stretching vibrations of O–H bonds in hydroxyl groups, whose presence can indicate the oxidation of mesoporous carbon surface and the presence of carboxyl or phenol oxygen groups [48,49]. For the oxidized materials, a new band appeared at about 1750 cm^{-1} , which was most pronounced for $C_{SBA-15-5-100}$. This band can be assigned to the carbonyl group of aldehyde, ester, or carboxyl acid. The most probable origin of this band is the presence of –COOH

groups on the surface of oxidized carbons, which is supported by the simultaneous presence of a band at about 3400 cm^{-1} [48,49]. The bands of the highest intensity were obtained for sample $C_{\text{SBA-15-5-100}}$, which has the highest content of functional acidic groups. The bands recorded for the other samples were less intensive because of the lower content of functional groups.

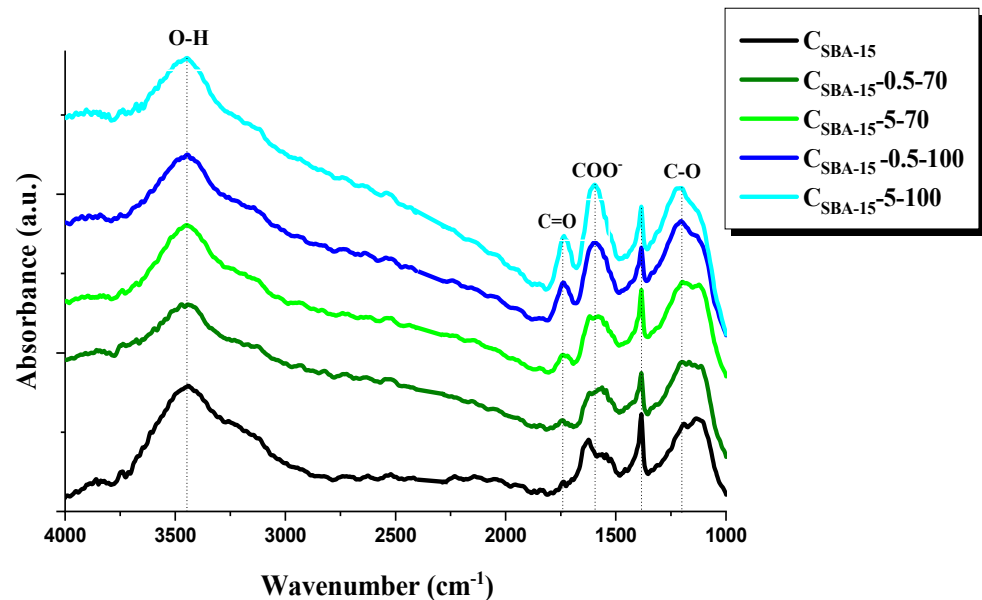


Figure 2. FT-IR spectra of carbon adsorbents obtained.

3.2. Adsorption Studies

In this work, we studied the kinetics of adsorption (Figure 3). The adsorption of rhodamine B on the surface of the carbon materials studied is very fast for the first 10 min. After this time, the majority of the active sites on the carbon surface is already occupied by the dye molecules and the rate of adsorption considerably decreases. After 1 h, no increase q_e was noted, which means that a state of equilibrium was reached and there are no more active sites on the carbon material studied. Next step, the experimental data were fitted to two kinetic models: pseudo-first-order (PFO) and pseudo-second-order models (PSO).

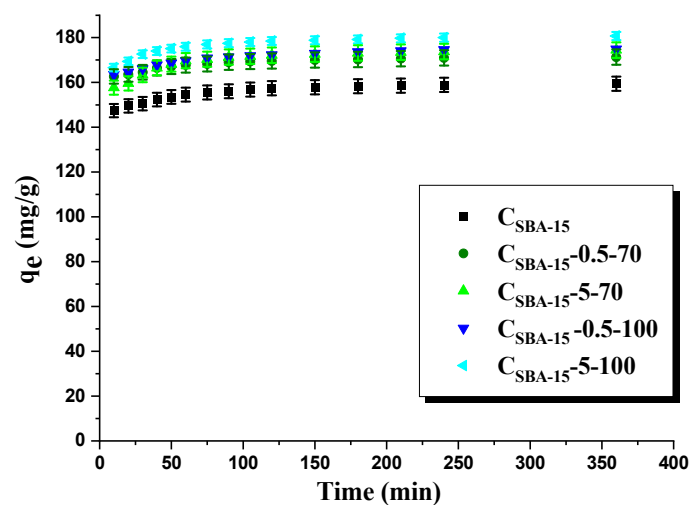


Figure 3. Amount of rhodamine B adsorbed on adsorbents obtained ($C_0=75\text{ mg/L}$).

According to data collected in Table 3, the R^2 for the PFO model takes values from the range 0.9265 to 0.9865. Much higher, and the same for all carbon material values of R^2 (0.9999), were obtained assuming the PSO model. Moreover, the sorption capacities

calculated assuming this model are mostly in agreement with their experimental values. Therefore, we conclude that the kinetics of rhodamine B adsorption on the surface of the samples studied can be described by the PSO model.

Table 3. Kinetic models parameters.

| Adsorbent | q_e (mg/g) | q_e [cal] (mg/g) | PFO Model | | PSO Model | | |
|-----------------------------|---------------|--------------------|----------------------------|----------------|--------------------|------------------|----------------|
| | | | k_1 (min ⁻¹) | R ² | q_e [cal] (mg/g) | k_2 (g/mg min) | R ² |
| C _{SBA-15} | 159.41 ± 3.19 | 9.94 | 0.019 | 0.9391 | 161.29 | 0.003 | 0.9999 |
| C _{SBA15-0.5-70} | 171.29 ± 3.43 | 7.35 | 0.018 | 0.9265 | 172.41 | 0.004 | 0.9999 |
| C _{SBA-15-5-70} | 174.46 ± 3.49 | 11.93 | 0.022 | 0.9253 | 175.44 | 0.003 | 0.9999 |
| C _{SBA-15-0.5-100} | 174.90 ± 3.49 | 11.44 | 0.026 | 0.9865 | 175.45 | 0.003 | 0.9999 |
| C _{SBA-15-5-100} | 180.71 ± 3.61 | 10.72 | 0.023 | 0.9687 | 181.81 | 0.003 | 0.9999 |

Figure 4 illustrates the effect of the adsorbate solution pH, changed in the range 2–12, on the amount of adsorbed rhodamine B, while Figure 5A presents the zeta potential curves vs. pH of mesoporous carbons before the dye adsorption, and Figure 5B, after its adsorption. As shown in Figure 5A, sample C_{SBA-15} has the isoelectric point (i_{ep}) at 3.4. The functionalization changes the adsorbents' surface, for C_{SBA-15-5-70} the isoelectric point is at pH 2.6 and for C_{SBA-15-5-100} it does not exist; the zeta potential in the whole range of measurement is negative. The negative zeta potential indicates that oxidation treatment with HNO₃ introduces hydroxyl, carboxylic, and carbonyl groups on the surfaces of the samples, which dissociate generating the negatively charged surface [50,51]. The zeta potential value higher than 25 mV, positive or negative, is indicative of electrokinetic stability [52]. Pristine carbon sample C_{SBA-15}, and the samples after oxidation (C_{SBA-15-5-70} and C_{SBA-15-5-100}), show good electrokinetic stability at pH values higher than 6 (Figure 5A). The data presented in Figure 4 suggest that the effectiveness of rhodamine B removal from water solutions depends on the pH of the adsorbate solution. The lowest sorption capacity was recorded at pH 2, which can be explained as a result of the protonation of carboxyl, amide, and hydroxyl groups, leading to the generation of a positive charge, which is engaged in repulsive interaction with the positive charge of the cationic dye (rhodamine B). In addition, at low pH, the H⁺ cations compete with rhodamine B cations for the adsorption sites. The surface is more negatively charged when the pH increases as a result of deprotonation of the functional groups by the hydroxide anion OH⁻, which is more favorable for the adsorption of rhodamine B. Then, we have strong electrostatic attraction between the negatively charged surface of the adsorbent and the positively charged cationic dye. At pH 12, the sorption capacities of all adsorbents increased by about 20 mg/g in relation to that of the initial carbon sample. The zeta potential values of C_{SBA-15-5-100} after adsorption of rhodamine B from the solutions of the concentration of 50 mg/L and 150 mg/L (Figure 5B) differ from those for C_{SBA-15-5-100} before adsorption, and i_{ep} can be observed (changes in i_{ep} value suggest the chemical adsorption) [53].

The effect of temperature on the amount of rhodamine B adsorbed on the surface of the samples studied was also checked (Figure 6). The amount of rhodamine B adsorbed (q_e) on the surface of mesoporous carbon materials before and after their oxidation increases with temperature. It follows the consequence of increased mobility of dye molecules at higher temperatures. For instance, the amount of organic dye adsorbed on the surface of sample C_{SBA-15-5-100} is 227 mg/g (25 °C), 254 mg/g (45 °C), and 261 mg/g (60 °C).

According to the data collected in Table 4, the results of ΔG° prove that the process of adsorption of dye is spontaneous. For all samples, the degree of spontaneity was the highest at 60 °C. The positive values of ΔH obtained reveal an endothermic adsorption process. In addition, the positive values of ΔS evidence increased the degree of randomness at the interface in the process of the rhodamine B adsorption.

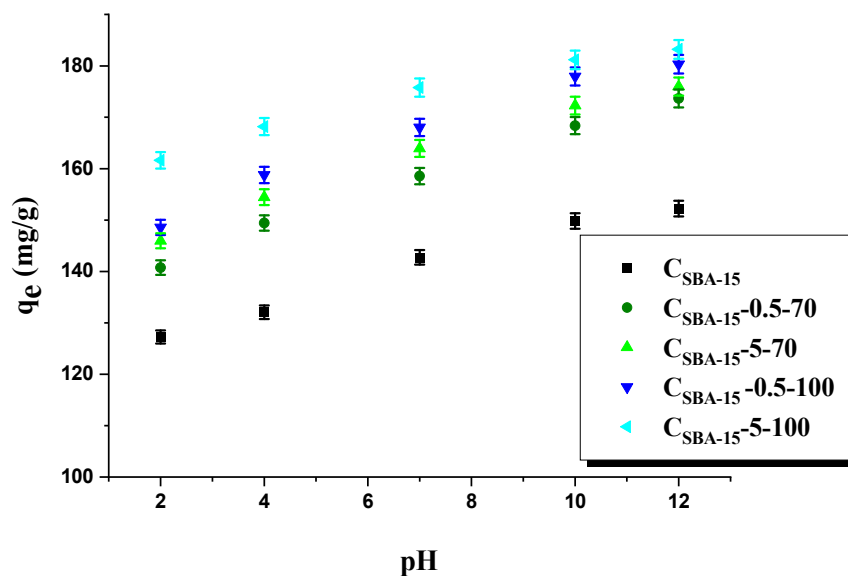


Figure 4. The pH influence on the sorption capacity of adsorbents obtained.

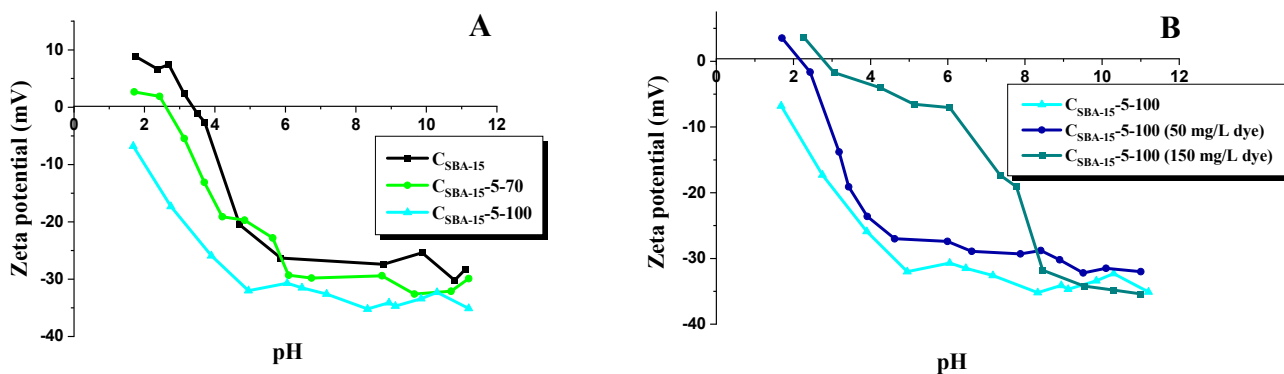


Figure 5. Zeta potential curves vs. pH for C_{SBA-15} , $C_{SBA-15-5-70}$, and $C_{SBA-15-5-100}$ mesoporous carbons before dye adsorption (A) and for C_{SBA-15} and $C_{SBA-15-5-100}$ after adsorption of rhodamine B (B).

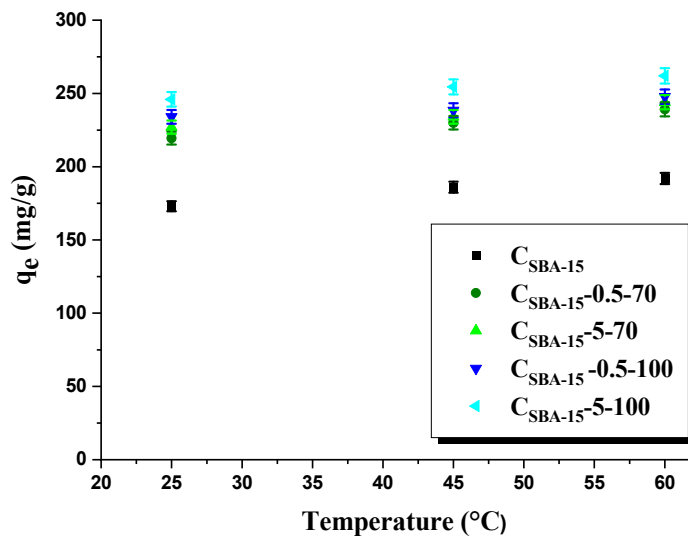
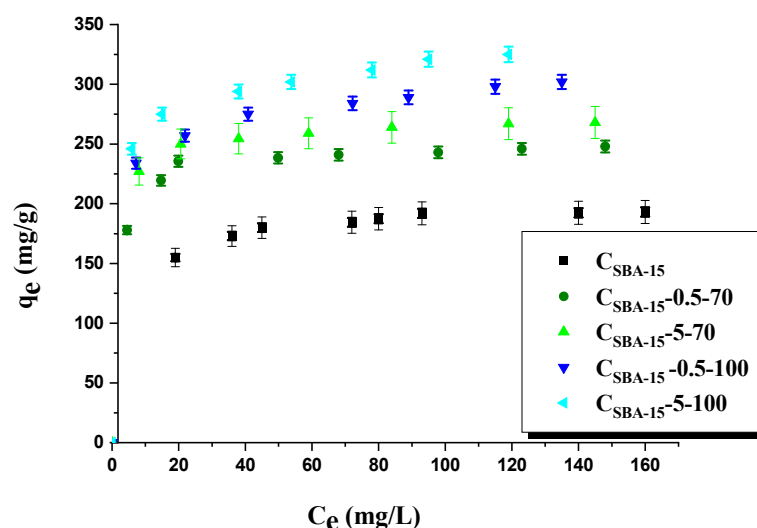


Figure 6. Effect of temperature on the adsorption of dye (100 mg/L) onto adsorbents obtained.

Table 4. Thermodynamic parameters obtained.

| Adsorbent | Temperature (°C) | ΔG^0 (kJ·mol ⁻¹) | ΔH^0 (kJ·mol ⁻¹) | ΔS^0 (J·mol ⁻¹ ·K ⁻¹) |
|-----------------------------|------------------|--------------------------------------|--------------------------------------|--|
| C _{SBA-15} | 25 | −16.41 | 31.20 | 159.71 |
| | 45 | −19.53 | | |
| | 60 | −22.01 | | |
| C _{SBA-15-0.5-70} | 25 | −19.51 | 23.96 | 145.66 |
| | 45 | −22.18 | | |
| | 60 | −24.51 | | |
| C _{SBA-15-5-70} | 25 | −22.27 | 22.44 | 149.90 |
| | 45 | −25.14 | | |
| | 60 | −27.53 | | |
| C _{SBA-15-0.5-100} | 25 | −19.12 | 43.69 | 210.76 |
| | 45 | −23.24 | | |
| | 60 | −26.51 | | |
| C _{SBA-15-5-100} | 25 | −21.66 | 47.17 | 230.88 |
| | 45 | −26.19 | | |
| | 60 | −29.73 | | |

Figure 7 presents the isotherms of dye adsorption on the surface of carbon adsorbents. According to the results, the initial carbon C_{SBA-15} proved to be the least effective in the removal of dye, despite having the largest surface area from among all samples studied (1203 m²/g). However, this material also has the lowest number of surface functional groups of acidic character. Further data analysis allows us to conclude that the process of the adsorption of organic dye depends on surface functional groups of acidic character. Sample C_{SBA-15-5-100}, showing the largest sorption capacity towards rhodamine B (325 mg/g), has the greatest content of such functional groups (4.88 mmol/g). The process of its oxidation was performed with 5 mol/L nitric (V) acid solution at 100 °C. The amounts of rhodamine B adsorbed on the other oxidized carbon materials C_{SBA-15-0.5-70}, C_{SBA-15-5-70}, and C_{SBA-15-0.5-100} were 248, 268, and 302 mg/g, respectively.

**Figure 7.** Adsorption of rhodamine B onto adsorbents obtained.

Analysis of the adsorption data was performed with the use of two theoretical models of Langmuir and Freundlich (Figures 8 and 9, Tables 5 and 6). Comparison of the experimental data with the predictions of a particular model provides information on the mechanism of adsorption and mesoporous carbon/rhodamine B interactions. The criterion of best fitting was the determination coefficient R².

The determination coefficient R^2 for the linear form of the Langmuir model takes values from 0.9987 to 0.9999 for all adsorbents obtained. The values of R^2 (Freundlich model) for particular carbon materials were: 0.8564 for C_{SBA-15} , 0.7993 for $C_{SBA-15-0.5-70}$, 0.8009 for $C_{SBA-15-5-70}$, 0.8611 for $C_{SBA-15-0.5-100}$, and 0.8598 for $C_{SBA-15-5-100}$. Therefore, the isotherms of rhodamine B adsorption on the surface of the carbon materials studied correspond to the Langmuir model. It should be noted that the experimental values of q_e are slightly lower from the theoretical q_m . For the oxidized mesoporous carbons, the coefficient K_L values are higher than for the initial material C_{SBA-15} , which means that the bonding between rhodamine B and the functionalized carbon material surfaces is stronger. The coefficient $1/n$ for the Freundlich model lies between ($0 < 1/n < 1$) which shows that this isotherm is favorable.

Table 5. The parameters of linear form of Langmuir and Freundlich models for rhodamine B adsorption onto carbon materials.

| Material | Langmuir | | | Freundlich | | |
|----------------------|--------------|--------------|--------|-------------------------------------|--------|--------|
| | q_m (mg/g) | K_L (L/mg) | R^2 | K_F (mg/g (L/mg) ^{1/n}) | 1/n | R^2 |
| C_{SBA-15} | 196.07 | 0.369 | 0.9999 | 102.48 | 0.1373 | 0.8564 |
| $C_{SBA-15-0.5-70}$ | 250.00 | 0.727 | 0.9998 | 119.92 | 0.1701 | 0.7993 |
| $C_{SBA-15-5-70}$ | 270.27 | 0.787 | 0.9998 | 127.98 | 0.1783 | 0.8009 |
| $C_{SBA-15-0.5-100}$ | 303.03 | 0.493 | 0.9988 | 141.83 | 0.1717 | 0.8611 |
| $C_{SBA-15-5-100}$ | 322.58 | 0.574 | 0.9987 | 153.34 | 0.1780 | 0.8598 |

Table 6. The parameters of non-linear Langmuir and Freundlich models for rhodamine B adsorption onto carbon materials.

| Material | Langmuir | | | Freundlich | | |
|----------------------|--------------|--------------|--------|-------------------------------------|--------|--------|
| | q_m (mg/g) | K_L (L/mg) | R^2 | K_F (mg/g (L/mg) ^{1/n}) | 1/n | R^2 |
| C_{SBA-15} | 200.64 | 0.179 | 0.9999 | 122.13 | 0.0949 | 0.8983 |
| $C_{SBA-15-0.5-70}$ | 248.73 | 0.566 | 0.9986 | 171.94 | 0.0793 | 0.8053 |
| $C_{SBA-15-5-70}$ | 268.28 | 0.660 | 0.9995 | 208.07 | 0.0530 | 0.9357 |
| $C_{SBA-15-0.5-100}$ | 296.66 | 0.454 | 0.9942 | 197.63 | 0.0860 | 0.9953 |
| $C_{SBA-15-5-100}$ | 319.83 | 0.505 | 0.9950 | 212.12 | 0.0897 | 0.9922 |

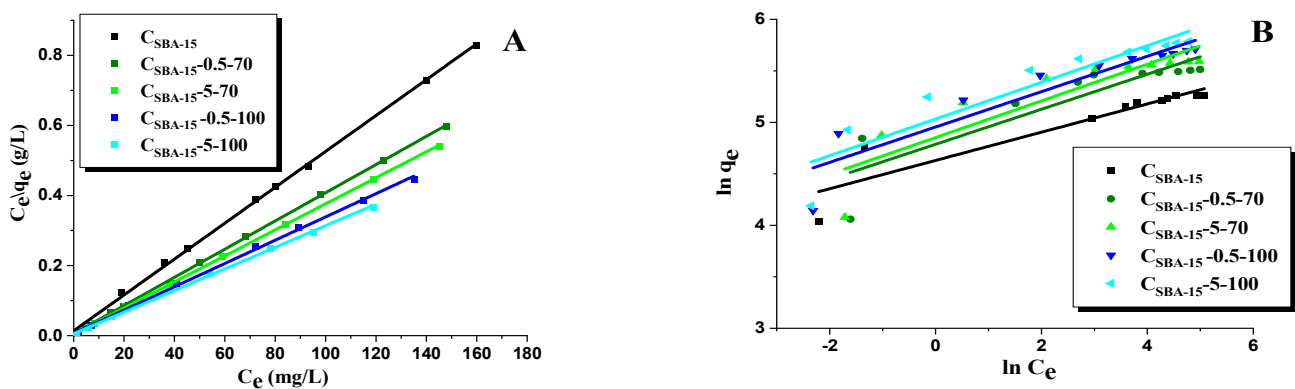


Figure 8. Linear fitting of rhodamine B adsorption isotherms onto carbon adsorbents to Langmuir (A) and Freundlich (B) models.

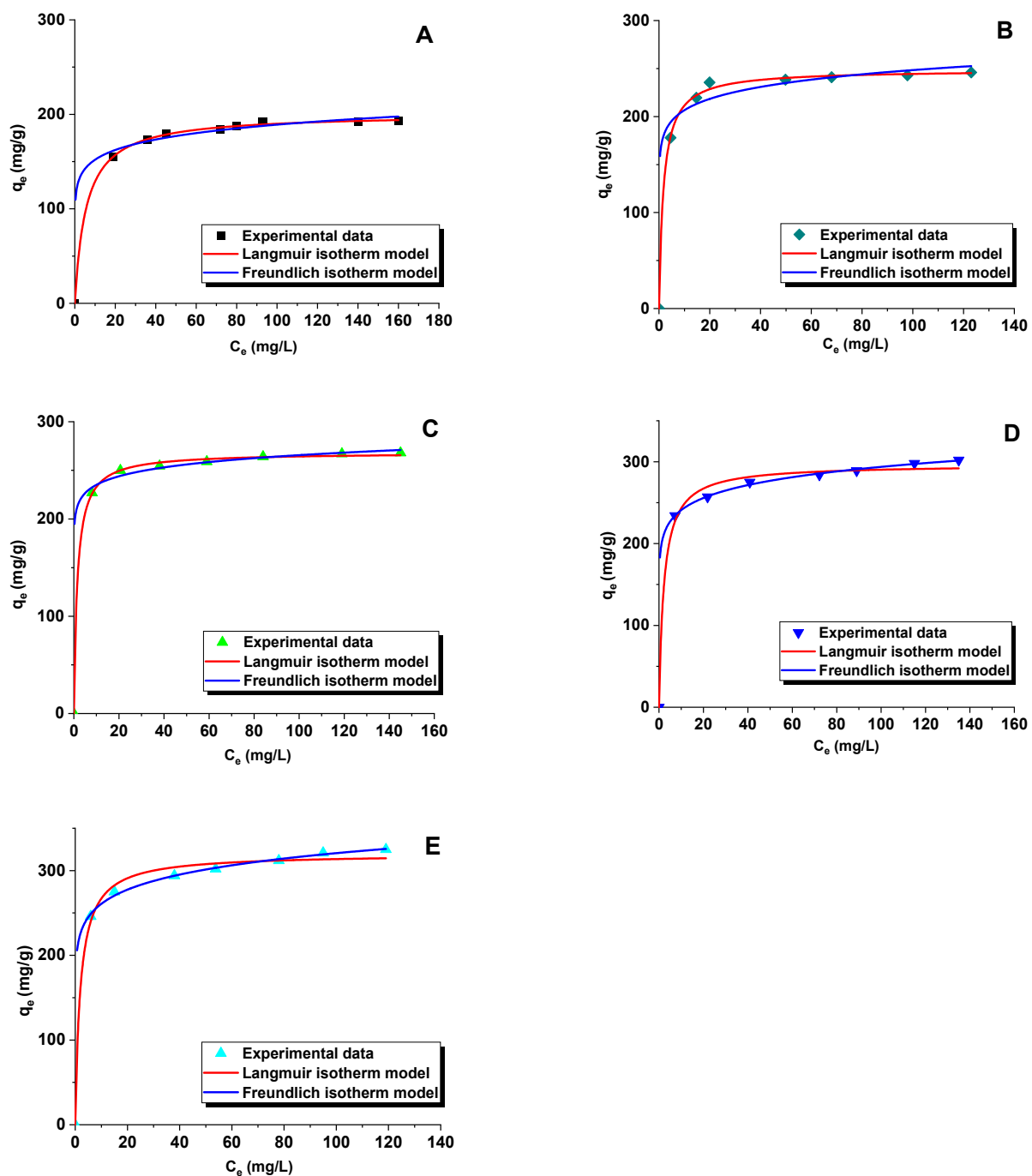


Figure 9. Non-linear fitting of rhodamine B adsorption isotherms to Langmuir and Freundlich models for samples: C_{SBA-15} (A), $C_{SBA15-0.5-70}$ (B), $C_{SBA-15-5-70}$ (C), $C_{SBA-15-0.5-100}$ (D), and $C_{SBA-15-5-100}$ (E).

Additionally, the comparison of the non-linear form of the Langmuir and the Freundlich [54] isotherm models with experimental data for the adsorption of rhodamine B on the surface of carbon adsorbents is presented in Table 6 and Figure 9. It was established that the Langmuir adsorption model indicates a better fit to the experimental data than the Freundlich model. The R^2 values for the non-linear and linear Langmuir isotherms were similar.

Table 7 presents a comparison of the sorption capacities of carbon samples obtained towards tested dye with those of other adsorbents. The comparison implies that the ordered mesoporous carbon materials are very effective in the removal of rhodamine B from

water solutions. The majority of literature reported adsorbents, including hierarchical SnS₂ nanostructure [5], TA-G [55], iron-pillared bentonite [56], sago waste activated carbon [57], kaolinite [58], [Ni_(bipy)]₂(HPW₁₂O₄₀) [59], orange peel [60], whose sorption capacities are lower than for the oxidized carbon materials studied in this work. From among all materials mentioned in Table 6, the highest sorption capacity towards rhodamine B showed the magnetic mesoporous carbon materials (342–400 mg/g) [61], also high sorption capacities were noted for MoS₂/MIL-101-345 mg/g [62] and oxidized ordered mesoporous carbon material C_{SBA-15-5-100} (325 mg/g). The hierarchical SnS₂ nanostructure [5] and TA-G [55] adsorption capacity was at a level of 200 mg/g, and the sorption capacities of the other samples listed in Table 7 were much lower: iron-pillared bentonite—99 mg/g [56], sago waste activated carbon—47 mg/g [57], kaolinite—46 mg/g [58], [Ni_(bipy)]₂(HPW₁₂O₄₀)—23 mg/g [59], and orange peel—14 mg/g [60].

Table 7. Comparison of sorption capacities of oxidized mesoporous carbons with other adsorbents presented in literature.

| Adsorbent | Sorption Capacity (mg/g) | References |
|---|--------------------------|------------|
| oxidized mesoporous carbon | 248–325 | This study |
| hierarchical SnS ₂ nanostructure | 200 | [5] |
| TA-G | 201 | [55] |
| iron-pillared bentonite | 99 | [56] |
| sago waste activated carbon | 47 | [57] |
| kaolinite | 46 | [58] |
| [Ni _(bipy)] ₂ (HPW ₁₂ O ₄₀) | 23 | [59] |
| orange peel | 14 | [60] |
| magnetic mesoporous carbon materials | 342–400 | [61] |
| MoS ₂ /MIL-101 | 345 | [62] |

4. Conclusions

According to the above-presented results, functionalization of the ordered mesoporous carbon of hexagonal structure (C_{SBA-15}) using a solution of nitric (V) acid, has brought about an increase in its effectiveness of rhodamine B removal from water solutions. Oxidization of mesoporous carbon reduced its textural parameters but increased the acidic character of the surface. Moreover, for the samples functionalized at 70 °C, the oxidation resulted in the disappearance of the reflections corresponding to the carbon structure ordering, as confirmed by XRD diffractograms in the small angle range. Sample C_{SBA-15-5-100} was characterized by the highest content of surface functional groups of acidic nature and the largest surface area from among the functionalized carbon materials studied. This sample was the most effective in the removal of tested dye from water solutions (325 mg/g). The sorption capacity towards rhodamine B depended also on the pH of the solution and the process temperature. The adsorption of organic dye was more effective at higher pH because of deprotonation of the surface functional groups on the carbon samples by the hydroxide anion. The measurements of zeta potential, before and after adsorption, proved that with increasing pH, the surface charge on carbon samples changed. The amount of adsorbed rhodamine B was also found to increase with the increasing temperature of the process, which is related to increased mobility of the dye molecules at higher temperatures. The thermodynamic parameters showed that the adsorption process of dye was endothermic and proceeded spontaneously. The adsorption of rhodamine B onto oxidized mesoporous carbons was described by the Langmuir isotherm and pseudo-second-order kinetic model.

Author Contributions: Conceptualization, M.M. and J.G.; methodology, M.M.; validation, M.M., J.G., M.N. and A.B.-W.; formal analysis, M.M. and J.G.; investigation, M.M., M.N. and A.B.-W.; resources, J.G., T.J. and R.P.; data curation, M.M.; writing—original draft preparation, M.M. and J.G.; writing—review and editing, M.M., J.G., M.N., T.J., A.B.-W. and R.P.; visualization, M.M. and J.G.; supervision, R.P.; funding acquisition, R.P. All authors have read and agreed to the published version of the manuscript.

Funding: This research received no external funding.

Institutional Review Board Statement: Not applicable.

Informed Consent Statement: Not applicable.

Data Availability Statement: Data is contained within the article.

Conflicts of Interest: The authors declare no conflict of interest.

References

1. Liu, R.C.; Zhang, B.; Mei, D.D.; Zhang, H.Q.; Liu, J.D. Adsorption of methyl violet from aqueous solution by halloysite nanotubes. *Desalination* **2011**, *268*, 111–116. [[CrossRef](#)]
2. Liang, Z.J.; Zhao, Z.W.; Sun, T.Y.; Shi, W.X.; Cui, F.Y. Enhanced adsorption of the cationic dyes in the spherical CuO/meso-silica nano composite and impact of solution chemistry. *J. Colloid Interf. Sci.* **2017**, *485*, 192–200. [[CrossRef](#)] [[PubMed](#)]
3. Hao, O.J.; Kim, H.; Chiang, P.C. Decolorization of wastewater. *Crit. Rev. Environ. Sci. Technol.* **2000**, *30*, 449–505. [[CrossRef](#)]
4. Bulai, I.M.; Venturino, E. Biodegradation of organic pollutants in a water body. *J. Math. Chem.* **2016**, *54*, 1387–1403. [[CrossRef](#)]
5. Wang, S.; Yang, B.; Liu, Y. Synthesis of a hierarchical SnS₂ nanostructure for efficient adsorption of Rhodamine B dye. *J. Colloid Interf. Sci.* **2017**, *507*, 225–233. [[CrossRef](#)] [[PubMed](#)]
6. Huang, Z.; Li, Y.; Chen, W.; Shi, J.; Zhang, N.; Wang, X.; Li, Z.; Gao, L.; Zhang, Y. Modified bentonite adsorption of organic pollutants of dye wastewater. *Mater. Chem. Phys.* **2017**, *202*, 266–276. [[CrossRef](#)]
7. Raman, C.D.; Kanmani, S. Textile dye degradation using nano zero valent iron: A review. *J. Environ. Manag.* **2016**, *177*, 341–355. [[CrossRef](#)]
8. Patil, S.P.; Bethi, B.; Sonawane, G.H.; Shrivastava, V.S.; Sonawane, S. Efficient adsorption and photocatalytic degradation of Rhodamine B dye over Bi₂O₃-bentonite nanocomposites: A kinetic study. *J. Ind. Eng. Chem.* **2016**, *34*, 356–363. [[CrossRef](#)]
9. Ptazkowska-Koniarz, M.; Goscińska, J.; Pietrzak, R. Adsorption of dyes on the surface of polymer nanocomposites modified with methylamine and copper(II) chloride. *J. Colloid Interf. Sci.* **2017**, *504*, 549–560. [[CrossRef](#)]
10. Li, S.; Jia, Z.; Li, Z.; Li, Y.; Zhu, R. Synthesis and characterization of mesoporous carbon nanofibers and its adsorption for dye in wastewater. *Adv. Powder Technol.* **2016**, *27*, 591–598. [[CrossRef](#)]
11. Firmino, P.I.M.; Da Silva, M.E.R.; Cervantes, F.J.; Dos Santos, A.B. Colour removal of dyes from synthetic and real textile wastewaters in one- and two-stage anaerobic systems. *Bioresour. Technol.* **2010**, *101*, 7773–7779. [[CrossRef](#)] [[PubMed](#)]
12. Cooper, C.; Burch, R. Mesoporous materials for water treatment processes. *Water Res.* **1999**, *33*, 3689–3694. [[CrossRef](#)]
13. Arshadi, M.; Mousavinia, F.; Amiri, M.J.; Faraji, A.R. Adsorption of methyl orange and salicylic acid on a nano-transition metal composite: Kinetics, thermodynamic and electrochemical studies. *J. Colloid Interf. Sci.* **2016**, *483*, 118–131. [[CrossRef](#)] [[PubMed](#)]
14. Errais, E.; Duplay, J.; Darragi, F. Textile dye removal by natural clay-case study of Fouchana Tunisian Clay. *Environ. Technol.* **2010**, *31*, 373–380. [[CrossRef](#)]
15. Marcucci, M.; Ciardelli, G.; Matteucci, A.; Ranieri, L.; Russo, M. Experimental campaigns on textile wastewater for reuse by means of different membrane processes. *Desalination* **2002**, *149*, 137–143. [[CrossRef](#)]
16. Alzahrani, S.; Mohammad, A.W. Challenges and trends in membrane technology implementation for produced water treatment: A review. *J. Water Process Eng.* **2014**, *4*, 107–133. [[CrossRef](#)]
17. Damodar, R.A.; You, S.; Ou, S. Coupling of membrane separation with photocatalytic slurry reactor for advanced dye wastewater treatment. *Sep. Purif. Technol.* **2010**, *76*, 64–71. [[CrossRef](#)]
18. Ou, W.; Zhang, G.; Yuan, X.; Su, P. Experimental study on coupling photocatalytic oxidation process and membrane separation for the reuse of dye wastewater. *J. Water Process Eng.* **2015**, *6*, 120–128. [[CrossRef](#)]
19. Kanagaraj, J.; Senthilvelan, T.; Panda, R.C. Degradation of azo dyes by laccase: Biological method to reduce pollution load in dye wastewater. *Clean. Technol. Environ. Policy* **2015**, *17*, 1443–1456. [[CrossRef](#)]
20. Kannan, C.; Sundaram, T.; Palvannan, T. Environmentally stable adsorbent of tetrahedral silica and non-tetrahedral alumina for removal and recovery of malachite green dye from aqueous solution. *J. Hazard. Mater.* **2008**, *157*, 137–145. [[CrossRef](#)]
21. Li, C.Z.; Zhong, H.; Wang, S.; Xue, J.R.; Zhang, Z.Y. Removal of basic dye (methylene blue) from aqueous solution using zeolite synthesized from electrolytic manganese residue. *J. Ind. Eng. Chem.* **2015**, *23*, 344–352. [[CrossRef](#)]
22. Dong, K.; Qiu, F.X.; Guo, X.R.; Xu, J.C.; Yang, D.Y.; He, K.C. Polyurethane-attapulgite porous material: Preparation, characterization, and application for dye adsorption. *J. Appl. Polym. Sci.* **2013**, *129*, 1697–1706. [[CrossRef](#)]
23. Goscińska, J.; Olejnik, A.; Pietrzak, R. In vitro release of L-phenylalanine from ordered mesoporous materials. *Micropor. Mesopor. Mater.* **2013**, *177*, 32–36. [[CrossRef](#)]

24. Derylo-Marczewska, A.; Marczewski, A.W.; Winter, S.; Sternik, D. Studies of adsorption equilibria and kinetics in the systems: Aqueous solution of dyes–mesoporous carbons. *Appl. Surf. Sci.* **2010**, *256*, 5164–5170. [[CrossRef](#)]
25. Goscińska, J.; Ptaszewska, M.; Pietrzak, R. Equilibrium and kinetic studies of chromotrope 2R adsorption onto ordered mesoporous carbons modified with lanthanum. *Chem. Eng. J.* **2015**, *270*, 140–149. [[CrossRef](#)]
26. Goscińska, J.; Marciniak, M.; Pietrzak, R. Ordered mesoporous carbons modified with cerium as effective adsorbents for azo dyes removal. *Sep. Purif. Technol.* **2015**, *154*, 236–245. [[CrossRef](#)]
27. Bazula, P.A.; Lu, A.H.; Nitz, J.T.; Schüth, F. Surface and pore structure modification of ordered mesoporous carbons via a chemical oxidation approach. *Micropor. Mesopor. Mater.* **2008**, *108*, 266–275. [[CrossRef](#)]
28. Liu, F.; Guo, Z.; Ling, H.; Huang, Z.; Tang, D. Effect of pore structure on the adsorption of aqueous dyes to ordered mesoporous carbons. *Micropor. Mesopor. Mater.* **2016**, *227*, 104–111. [[CrossRef](#)]
29. Asouhidou, D.D.; Triantafyllidis, K.S.; Lazaridis, N.K.; Matis, K.A.; Kim, S.S.; Pinnavaia, T.J. Sorption of reactive dyes from aqueous solutions by ordered hexagonal and disordered mesoporous carbons. *Micropor. Mesopor. Mater.* **2009**, *117*, 257–267. [[CrossRef](#)]
30. Peng, X.; Hu, X.; Fu, D.; Lam, F.L.Y. Adsorption removal of acid black 1 from aqueous solution using ordered mesoporous carbon. *Appl. Surf. Sci.* **2016**, *294*, 71–80. [[CrossRef](#)]
31. Cai, T.; Liu, Y.; Wang, L.; Dong, W.; Chen, H.; Zeng, W.; Xia, X.; Zeng, G. Activation of persulfate by photoexcited dye for antibiotic degradation: Radical and nonradical reactions. *Chem. Eng. J.* **2019**, *375*, 122070. [[CrossRef](#)]
32. Sulistina, D.R.; Martini, S. The effect of Rhodamine B on the cerebellum and brainstem tissue of *Rattus norvegicus*. *J. Public Health Res.* **2020**, *9*, 1812. [[CrossRef](#)]
33. Chen, L.; Liu, H.; Ren, X. Synthesis and characterization of magnetic metal–organic framework for the adsorptive removal of rhodamine B from aqueous solution. *J. Ind. Eng. Chem.* **2016**, *34*, 278–285. [[CrossRef](#)]
34. Deng, J.; Chen, Y.J.; Lu, Y.A.; Ma, X.Y.; Feng, S.F.; Gao, N.; Li, N. Synthesis of magnetic CoFe₂O₄/ordered mesoporous carbon nanocomposites and application in Fenton-like oxidation of rhodamine B. *Environ. Sci. Pollut. Res.* **2017**, *24*, 14396–14408. [[CrossRef](#)] [[PubMed](#)]
35. Moradi, S.E.; Nasrollahpour, A. Competitive adsorption and photodegradation of Methyl orange and Rhodamine B by TiO₂ modified mesoporous carbon photo-catalyst on UV irradiation. *Mater. Technol.* **2017**, *32*, 716–723. [[CrossRef](#)]
36. Tripathi, N.K. Porous carbon spheres: Recent developments and applications. *AIMS Mater. Sci.* **2018**, *5*, 1016–1052. [[CrossRef](#)]
37. Zhao, D.; Huo, Q.; Feng, J.; Chmelka, B.F.; Stucky, G.D. Nonionic triblock and star diblock copolymer and oligomeric surfactant syntheses of highly ordered hydrothermally stable mesoporous silica structures. *J. Am. Chem. Soc.* **1998**, *120*, 6024–6036. [[CrossRef](#)]
38. Zhao, D.; Feng, J.; Huo, Q.; Melosh, N.; Fredrickson, G.H.; Chmelka, B.F.; Stucky, G.D. Triblock copolymer syntheses of mesoporous silica with periodic 50 to 300 angstrom pores. *Science* **1998**, *279*, 548–552. [[CrossRef](#)]
39. Joo, H.; Choi, J.; Oh, I.; Kwak, J.; Liu, Z.; Terasaki, O.; Ryoo, R. Ordered nanoporous arrays of carbon supporting high dispersions of platinum nanoparticles. *Nature* **2001**, *412*, 169–172. [[CrossRef](#)]
40. Boehm, H.P. Some aspects of the surface chemistry of carbon blacks and other carbons. *Carbon* **1994**, *32*, 759–769. [[CrossRef](#)]
41. Olejnik, A.; Goscińska, J. On the importance of physicochemical parameters of copper and aminosilane functionalized mesoporous silica for hydroxychloroquine release. *Mater. Sci. Eng. C* **2021**, *130*, 112438. [[CrossRef](#)] [[PubMed](#)]
42. Nashine, A.L.; Tembhurkar, A.R. Equilibrium, kinetic and thermodynamic studies for adsorption of As(III) on coconut (*Cocos nucifera* L.) fiber. *J. Environ. Chem. Eng.* **2016**, *4*, 3267–3273. [[CrossRef](#)]
43. Konggidinata, M.I.; Chao, B.; Lian, Q.; Subramaniam, R.; Zappi, M.; Gang, D.D. Equilibrium, kinetic and thermodynamic studies for adsorption of BTEX onto Ordered Mesoporous Carbon (OMC). *J. Hazard. Mater.* **2017**, *336*, 249–259. [[CrossRef](#)] [[PubMed](#)]
44. Dursun, A.Y.; Kalayci, C.S. Equilibrium, kinetic and thermodynamic studies on the adsorption of phenol onto chitin. *J. Hazard. Mater.* **2005**, *123*, 151–157. [[CrossRef](#)] [[PubMed](#)]
45. Langmuir, I. The constitutional and fundamental properties of solids and liquids. *J. Am. Chem. Soc.* **1916**, *38*, 2221–2295. [[CrossRef](#)]
46. Freundlich, H. Über die Adsorption in Lösungen. *Z. Phys. Chem.* **1907**, *57*, 385–470. [[CrossRef](#)]
47. Wu, Z.; Webley, P.A.; Zhao, D. Comprehensive Study of Pore Evolution, Mesostructural Stability, and Simultaneous Surface Functionalization of Ordered Mesoporous Carbon (FDU-15) by Wet Oxidation as a Promising Adsorbent. *Langmuir* **2010**, *26*, 10277–10286. [[CrossRef](#)]
48. Cohn, A.P.; Erwin, W.R.; Share, K.; Oakes, L.; Westover, A.S.; Carter, R.E.; Bardhan, R.; Pint, C.L. All Silicon Electrode Photocapacitor for Integrated Energy Storage and Conversion. *Nano Lett.* **2015**, *15*, 2727–2731. [[CrossRef](#)]
49. Prahaz, D.; Kartika, Y.; Indraswati, N.; Ismadji, S. Activated carbon from jackfruit peel waste by H₃PO₄ chemical activation: Pore structure and surface chemistry characterization. *Chem. Eng. J.* **2008**, *140*, 32–42. [[CrossRef](#)]
50. Li, Y.; Dua, Q.; Liua, T.; Peng, X.; Wang, J.; Sun, J.; Wang, Y.; Wu, S.; Wang, Z.; Xia, Y.; et al. Comparative study of methylene blue dye adsorption onto activated carbon, graphene oxide, and carbon nanotubes. *Chem. Eng. Res. Des.* **2013**, *91*, 361–368. [[CrossRef](#)]
51. Galán, J.; Rodríguez, A.; Gómez, J.M.; Allen, S.J.; Walker, G.M. Reactive dye adsorption onto a novel mesoporous carbon. *Chem. Eng. J.* **2013**, *219*, 62–68. [[CrossRef](#)]
52. Goscińska, J.; Olejnik, A.; Nowak, I. APTES-functionalized mesoporous silica as a vehicle for antipyrine–adsorption and release studies. *Colloid Surf. A* **2017**, *533*, 187–196. [[CrossRef](#)]

53. Dawood, S.; Sen, T.K.; Phan, C. Synthesis and Characterisation of Novel-Activated Carbon from Waste Biomass Pine Cone and Its Application in the Removal of Congo Red Dye from Aqueous Solution by Adsorption. *Water Air Soil Pollut.* **2014**, *225*, 1818. [[CrossRef](#)]
54. Alswieleh, A.M. Efficient Removal of Dyes from Aqueous Solution by Adsorption on L-Arginine-Modified Mesoporous Silica Nanoparticles. *Processes* **2022**, *10*, 1079. [[CrossRef](#)]
55. Liu, K.; Li, H.; Wang, Y.; Gou, X.; Duan, Y. Adsorption and removal of rhodamine B from aqueous solution by tannic acid functionalized graphene. *Colloid Surf. A Physicochem. Eng. Asp.* **2015**, *477*, 35–41. [[CrossRef](#)]
56. Hou, M.F.; Ma, C.X.; Zhang, W.D.; Tang, X.Y.; Fan, Y.N.; Wan, H.F. Removal of rhodamine B using iron-pillared bentonite. *J. Hazard. Mater.* **2011**, *186*, 1118–1123. [[CrossRef](#)]
57. Kadirvelu, K.; Karthika, C.; Vennilamani, N.; Pattabhi, S. Activated carbon from industrial solid waste as an adsorbent for the removal of rhodamine-B from aqueous solution: Kinetic and equilibrium studies. *Chemosphere* **2005**, *60*, 1009–1017. [[CrossRef](#)]
58. Khan, T.A.; Dahiya, S.; Ali, I. Use of kaolinite as adsorbent: Equilibrium, dynamics and thermodynamic studies on the adsorption of Rhodamine B from aqueous solution. *Appl. Clay Sci.* **2012**, *69*, 58–66. [[CrossRef](#)]
59. Li, F.; Chen, Y.; Huang, H.; Cao, W.; Li, T. Removal of rhodamine B and Cr(VI) from aqueous solutions by a polyoxometalate adsorbent. *Chem. Eng. Res. Des.* **2015**, *100*, 192–202. [[CrossRef](#)]
60. Annadurai, G.; Juang, R.S.; Lee, D.J. Use of cellulose-based wastes for adsorption of dyes from aqueous solutions. *J. Hazard. Mater.* **2002**, *92*, 263–274. [[CrossRef](#)]
61. Dong, Y.; Lin, H.; Qu, F. Synthesis of ferromagnetic ordered mesoporous carbons for bulky dye molecules adsorption. *Chem. Eng. J.* **2012**, *193–194*, 169–177. [[CrossRef](#)]
62. Yang, C.; Cheng, J.; Chen, Y.; Hu, Y. Enhanced adsorption performance of MoS₂ nanosheet-coated MIL-101 hybrids for the removal of aqueous rhodamine B. *J. Colloid Interface Sci.* **2017**, *504*, 39–47. [[CrossRef](#)] [[PubMed](#)]